Spatially resolved transcriptomics reveals plant host responses to pathogens

Michael Giolai[1,2], Walter Verweij[2,3], Ashleigh Lister[2], Darren Heavens[2], Iain Macaulay[2] and Matthew D. Clark[2,4 *]

[1] John Innes Centre, Norwich Research Park, Norwich, UK

[2] Earlham Institute, Norwich Research Park, Norwich, UK

[3] Enza Zaden, Enkhuizen, NL

[4] Natural History Museum, London, UK

Address correspondence to Matthew Clark, Natural History Museum, London, UK; E-mail: matt.clark@nhm.ac.uk

Abstract

Thorough understanding of complex model systems requires the characterisation of processes in different cell types of an organism. This can be achieved with high-throughput spatial transcriptomics at a large scale. However, for plant model systems this is still challenging as suitable transcriptomics methods are sparsely available. Here we present Grid-seq, an easy to adopt, micro-scale spatial-transcriptomics workflow that allows to study expression profiles across small areas of plant tissue at a fraction of the cost of existing sequencing-based methods. To benchmark Grid-seq, we compare the method with widely used library preparation methods (Illumina TruSeq). In spatial experiments we show that the Grid-seq method is sensitive enough to identify expression differences across a plant organ. We further assess the spatial transcriptome response of *Arabidopsis thaliana* leaves exposed to the bacterial molecule flagellin-22. In a series of RNA-seq experiments we show that our method can be used to identify known, rapidly flagellin-22 elicited genes, plant immune response pathways to bacterial attack and spatial expression patterns of genes associated with these pathways.

Key words:

Spatial transcriptomics, transcriptomics, transcriptome landscape, RNA-seq, plant immunity, plant defence response, flg22, biotic interaction, Grid-seq

Background

Most model plants and all crops species are multicellular, consisting of multiple organs and cell types with a multitude of physiological states [1]. A thorough understanding of these complex systems requires the ability to dissect and characterise processes in the different organs and cell types. This is challenging, though recently multi-omics single-cell studies have been flourishing [2], but high-throughput, high-resolution methodologies that assess molecular conditions with spatial resolution are sparsely available [3–6].

Although some spatial and low-input transcriptome profiling methods have been developed for animal model organisms [3–5,7], these methods are difficult to transfer to plants [6,8]. In comparison to animal cells, plant tissues hold a series of additional challenges: the robust plant cell wall requires specialised sample preparation (which makes reproducible, high-throughput sample preparation more difficult) and some plant secondary metabolites e.g. polyphenols can inhibit downstream enzymatic processes [9].For plants, single plant cells (protoplasts) can be obtained by enzymatic removal of plant-cell walls and subsequent fluorescent activated cell sorting (FACS) assays [10]. At the sub-cellular scale plant nuclei can be isolated within minutes by cell lysis and FACS [10–12]. However, 'stimulus and response' assays, such as differential gene-expression experiments or the characterisation of cell-type transcripts could be affected by these additional experimental procedures before RNA-extraction. Another important factor is the loss of spatial information when nuclei or protoplasts are extracted from a tissue. Thus methods such as fluorescent in-situ hybridisation (FISH) [13], laser-capture microdissection (LCM) [14–16] or the SPATiAL TRANSCRIPTOMICS [4,6] workflow are better suited to understand spatial transcription changes. However, all three methods need specific tissue preparations (e.g. cryo-sectioning, permeabilization or fixation) and specialised protocols to assess transcriptome levels: FISH methods require imaging of

49 transcripts and are restricted to multiplexing a few fluorescent anti-sense probes at a time [3], LCM
50 requires specialised equipment and training for precise, laborious excision of specific tissue elements
51 [6] and the SPATiAL TRANSCRIPTOMICS protocol requires preparation of thinly sectioned,
52 permeabilised samples and custom made DNA arrays [4,6].

53 Despite the high level of resolution that can be achieved with all these methods, they are not easily
54 applied in most laboratories. We aimed to overcome this with our Grid-seq workflow. Grid-seq is
55 designed to quickly process mechanically dissected samples into sequencing libraries using standard
56 laboratory equipment and can be used in most modern laboratories. Grid-seq is based on three
57 consecutive steps: (1) rapid, mechanical sample dissection of small e.g. 1 mm^2 leaf areas, (2) a high-
58 throughput method for high quality mRNA extraction of difficult to lyse plant tissues and (3) next
59 generation sequencing (NGS) library construction (**Figure 1**).

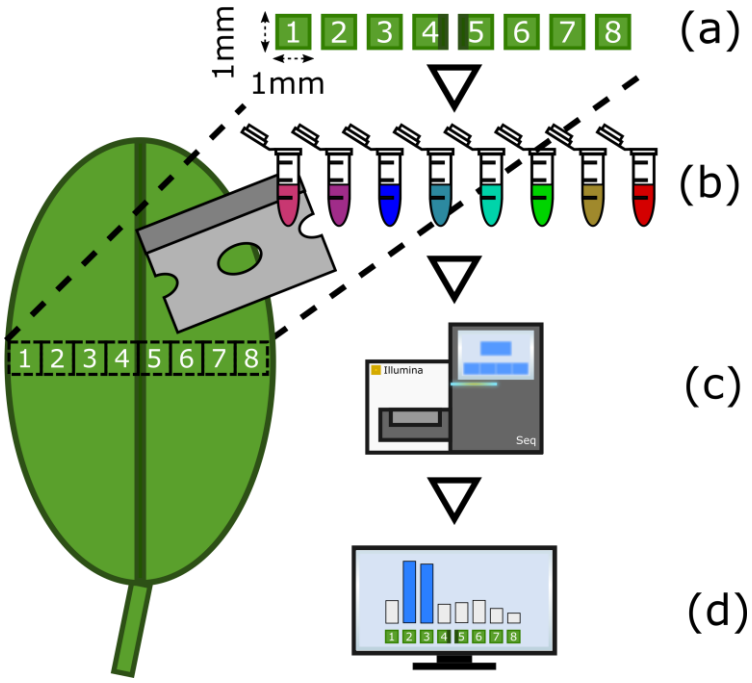

60

61 **Figure 1 Overview of the Grid-seq workflow:** (a) Tissue sections of approximately 1 mm^2 size are mechanically extracted
62 (e.g. a cross-section of a leaf) and after mRNA extraction (b) prepared into uniquely barcoded Illumina sequencing libraries.
63 After (c) Illumina sequencing (d) transcript specific, spatial expression data can be assessed and analysed.

64 In a series of experiments, we compare the performance of Grid-seq with standard RNA-seq (Illumina
65 TruSeq) experiments. Using Illumina sequencing we identify differentially expressed (DE) genes in 1D
66 (across lateral leaf sections) observing how transcripts and expression levels vary across the tissues
67 that make up the leaf organ. We compare large-scale vs. fine-scale transcriptome experiments ability
68 to detect plant responses induced by the bacterial peptide flagellin-22 (flg22), a well-described
69 pathogen-associated molecular pattern (PAMP) that triggers plant immune responses [17]. By
70 comparing our data with published datasets for 'flagellin rapidly elicited' (FLARE) genes [18] we
71 identified 143 of 253 described FLARE genes that overlap with our data, and a further 428 genes with
72 similar expression patterns to FLARE genes. We show that the detected 428 transcripts, are enriched
73 for plant defence responses and that spatial transcriptome data can be used to reconstruct the
74 spatial expression of pathway components across leaves. In additional pilot experiments using
75 *Arabidopsis thaliana* and the oomycete pathogen *Albugo laibachii* we also show that the dual dataset
76 of both host and pathogen, are captured, and spatial expression profiles can be constructed which
77 could be used to study the biotic interactions in infections

78 **Results**

79 **Does leaf dissection induce wounding response gene expression profiles?**

80 Physical wounding of plants is known to induce wounding related gene expression [19]. This is an
81 important point to consider as the Grid-seq workflow dissects tissue into ~ 1 mm^2 squares followed
82 by immediate snap freezing on dry ice. Yet dissection could potentially lead to activation of wounding
83 related gene expression and dissection takes longer as the resolution increases (grid size). As any
84 wounding effect could form a technical limitation to Grid-seq we measured the number of DE-genes
85 found after tissue dissection. For this we prepared ~1 mm^2 leaf squares (3 biological replicates per
86 time-point) at the time-points: 0-minutes, 2.5-minutes, 5-minutes and 10-minutes between cutting
87 and freezing on dry ice (when all enzymatic reactions cease). To determine the number of DE-genes
88 at each time-point we compared the 2.5-minute, 5-minute and 10-minute samples with the 0-minute

89 samples as an unwounded reference. This analysis showed just 1 DE-gene (AT2G37130) at the 2.5-
90 minute time-point (which was not significant at later time-points) there were no DE-genes at the 5-
91 minute time-point and 13 genes at the 10-minute time-point (see: **Additional_file1.docx** and
92 **Additional_file2.xlsx**) suggesting that the transcriptional response to wounding starts between 5 and
93 10 minutes. We looked for enriched biological processes in the combined set of 14 genes and
94 detected three genes at the 10-minute time-point being associated with the GO-term 'response to
95 wounding': *TPS04, TAT3* and AT1G62660 (see: **Additional_file1.docx** and **Additional_file2.xlsx**). This
96 indicates that it is highly desirable to cut and snap freeze sample material within 10 minutes to avoid
97 perturbation of results – a time window in which we find that sample dissection is easily achievable.

98 **Spatially resolved transcriptomics data reveals leaf tissue specific gene expression**

99 We assayed Grid-seq's ability to detect known gene expression differences between tissue types in
100 untreated leaves. Briefly, we dissected a lateral cross-section of an *A. thaliana* leaf (3 biological
101 replicates) into a 1-dimensional (1D) expression map of eight circa1 mm^2 squares (**Figure *2*A**)**.** Each
102 cross-section was sampled according to the same pattern: the leaf margins were located at square-1
103 and square-8 and the midvein at square-5. We then identified DE-genes by comparing the midvein
104 with the lamina and the leaf margins with the lamina. This resulted in 393 DE-genes for the midvein
105 and 686 DE-genes for the leaf margins comparison (**Figure 2** and file: **Additional_file2.xlsx**).

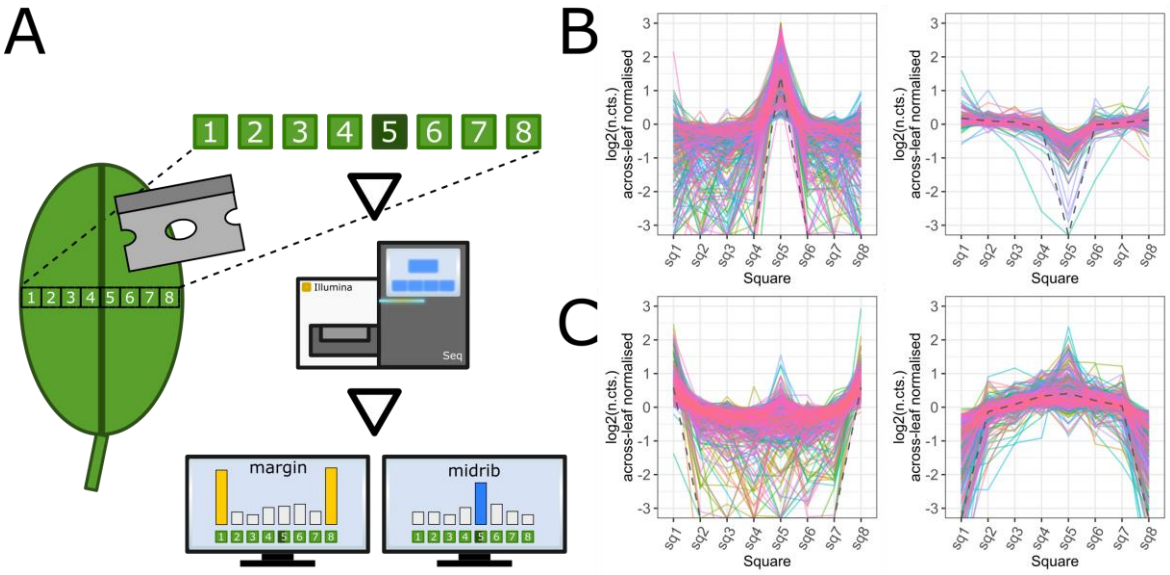

Figure 2 Identification of midvein and edge DE-genes in a lateral 1D leaf cross-section: (A) DE-gene analysis of a 1D *A. thaliana* leaf lateral cross sections by comparing the midvein (square-5) or the margin squares (square-1 and square-8) with the 'bulk' (remaining) leaf sections. The two images in (B) show 393 DE-genes with higher (left, 256 DE genes) or lower (right, 137 DE genes) expression values in the midvein. The images in (C) show 686 DE-genes higher (left, 403 DE genes) or lower (right, 283 DE genes) expression in the leaf margins. The grey dashed line in each plot (B and C) represents a trend-line for the average log2(counts) of all genes normalised across the leaf squares.

Comparison of spatial and bulk transcriptomics after localised flg22 stimulation

To compare spatial (only treated areas) with bulk (large leaf areas with treated and untreated areas) PAMP immune responses we used a flg-22 syringe infiltration assay. For this we produced small, local infiltration spots on the abaxial, left-hand side of a leaf of 6 biological *A. thaliana* replicates using either 500 nM flg22 or water (**Figure 3A**). We incubated the plants for 1 hour and sampled by dissecting leaf samples with a 1D system as above, briefly: square-1 (in the middle of the left half of a leaf) as infiltration spot and then laterally towards the midvein square-2 as non-vascular leaf tissue, square-3 as the midvein and square-4 as non-vascular leaf tissue.

In our analysis we wanted to measure how bulk RNA-seq datasets compared to spatially collected ones by using the number of detectable DE-genes. We hypothesised that the spatial analysis of the small, local treatment spot (square-1) and its surroundings (square-2, square-3 and square-4) would reveal more and distinct types (or waves) of flg22 responsive DE-genes than a bulk analysis would –

especially of rarer transcripts. To measure the effect of spatial information alone we simulated an *in silico* flg22 bulk experiment by combining the data from flg22 or water treated square-1 with the other untreated squares-2, 3 and 4 of the same leaf. We then called the treatment responsive DE-genes from the bulk files, detecting 65 DE-genes (39 higher expressed, 26 lower expressed) 1 hour after flg22 infiltration. We detected 887 more DE-genes (952 in total) by comparing the single squares of the flg22 and water infiltration dataset: 646 DE-genes for square-1 (416 higher, 230 lower expressed), 401 DE-genes for square-2 (306 higher, 95 lower expressed), 9 DE-genes for square-3 (8 higher, 1 lower expressed) and any DE-genes for square-4 (see: **Additional_file2.xlsx**). In contrast comparing the gene lists of the *in silico* bulk and spatial analysis we detected that 4 DE-genes were exclusively called from the bulk dataset and 64 genes were shared by both datasets.

To identify the biological processes uncovered by our transcriptomics experiments we performed a GO-term enrichment analysis the spatial flg22 related DE-gene datasets. From all (952) DE-genes we obtained 168 enriched GO-terms; among them we observed a high number of biological processes related to stress and defence responses (see: **Figure 3B**).

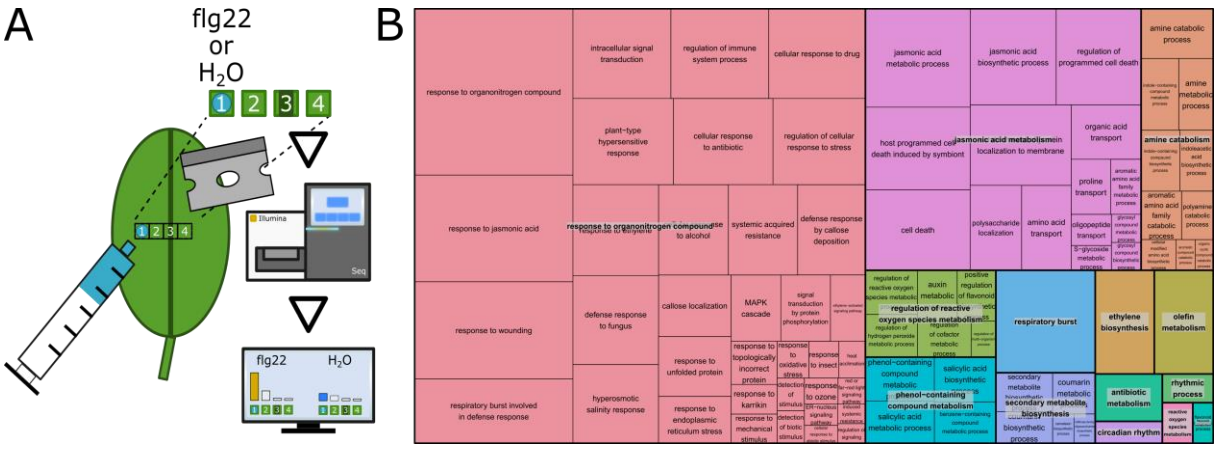

Figure 3 Elicitation of early *A. thaliana* defence response genes by infiltrating the bacterial peptide flg22: (A) To provide a strong stress stimulus we used syringe infiltration of either 500 nM flg22 or, as a control, water on a small area of the abaxial side of a leaf (square-1). 1 hour after infiltration we dissected 4 squares of a lateral leaf section with square-1 being the infiltration spot, square-2 and square-4 untreated, non-vascular leaf tissue and square-3 as midvein. The figure in (B) shows the REVIGO *[20]* treemap of the detected 168 GO-terms grouped under parent terms such as 'response to organonitrogen compound' (rose), 'jasmonic acid metabolism' (purple), 'amine catabolism' (orange) 'regulation of reactive

146 oxygen species metabolism' (green), 'phenol-containing compound metabolism' (azure blue), 'respiratory burst' (blue), etc..
147 The size of each rectangle relates to the absolute log10(q-value) – the larger the more significant.

148 **Early elicited flg22 response genes of local, fine-scale stimulation**

149 To simulate an initial pathogen encounter we used a milder stimulus method than the above
150 described syringe infiltration: we prepared 6 biological *A. thaliana* replicates by depositing 1 µl of 500
151 nM flg22 on square-3 of the abaxial side of a leaf and 1 µl of water (internal control) on square-6
152 (equivalent locations due to leaf bilateral symmetry). After one hour we extracted the treated leaf
153 area as a 1D lateral cross-section containing 8 separate 1 mm^2 squares (**Figure 4A**). We were
154 interested in DE-genes at the site of flg22 spotting (square-3) and in adjacent sections (square-2 and
155 square-4) as we reasoned that the plant would respond to the PAMP locally at first and then
156 responses via signalling to adjacent tissues and the rest of the plant. We called DE-genes by
157 comparing the flg22 with the water droplet spots (square-3 vs square-6) and the adjacent sections
158 with their corresponding bilateral equivalents (square-2 vs square-7 and square-4 vs square-5). Due
159 to the milder stimulus in comparison to the flg22 infiltration dataset we expected the number of DE-
160 genes could be lower than in the syringe infiltration experiment where we detected 952 DE genes.
161 Indeed, we identified a lower number of 523 DE-genes (491 higher expressed, 32 lower expressed)
162 for the droplet spot, and 5 DE-genes in the adjacent sections (1 higher expressed DE-gene in the
163 square-4 square-5 comparison and 4 higher expressed DE-genes in the square-2 vs square 7
164 comparison). Thus, in total we detected 526 individual DE-genes.

165 We compared both droplet spotting and syringe infiltration datasets (each dataset was collected 1
166 hour after flg22 exposure) for biological processes using GO-term enrichment. Both experiments
167 produced a similar number of enriched GO-terms with 159 biological processes enriched in the
168 droplet spotting dataset and 168 biological processes enriched in the infiltration dataset, with an
169 overlap of 132 biological processes (83.0 % of the spotting dataset and 78.5 % of the infiltration
170 dataset) between both datasets (see: **Additional_file2.xlsx**). The percentage of shared, enriched GO-

171 terms indicated the presence of a similar plant response to flg22 in both experiments despite the
172 difference in stimulus strength.

173 We measured the DE-genes with the 253 flagellin rapidly elicited (FLARE) genes described by seedling
174 and cell culture flg22 exposure experiment of Navarro et al. [18] (see: **Additional_file2.xlsx**). We
175 found that the DE-genes of the droplet spotting experiment contained 24.90 % FLARE genes (63 of
176 253 genes). These consisted of 32 FLARE genes associated with signal transduction, 11 genes
177 associated with roles in signal perception, 14 with known or putative roles as effector proteins and 9
178 FLARE genes identified by Navarro et al. as 'other' FLAREs (see: **Additional_file2.xlsx**). We found a
179 slightly higher number in the infiltration experiment: 80 DE genes were shared with the 253 FLARE
180 genes (31.62 %) with 39 genes associated with signal transduction, 16 genes in signal perception, 15
181 genes with known or putative roles as effector proteins and 11 genes with other functions (see:
182 **Additional_file2.xlsx**). Interestingly the % of known FLARE and the number of enriched biological
183 processes was higher in the infiltration than the spotting experiment (possibly suggesting other
184 processes are triggered by infiltration).

185 We were interested in the spatial expression patterns of the 63 shared FLARE genes between our
186 droplet spotting experiment and the Navarro et al. dataset. For this we visualised the expression
187 patterns of the FLAREs across the studied leaf area. All 63 FLARE genes showed high expression levels
188 at the area of flg22 exposure in comparison to adjacent leaf squares (Figure 5**B**). To study the
189 expression profiles of the remaining 460 DE genes identified in the flg22 droplet spotting experiment,
190 we affinity propagation clustered [21] these DE genes based on their spatial expression patterns and
191 visualised the expression profile of each cluster (**Figure 4C**). We identified three gene clusters: two of
192 the three clusters contained genes with higher expression levels at or adjacent to the area of flg22
193 treatment and one cluster contained a group of lower expressed genes at the flg22 treated area
194 (**Figure 4C**).

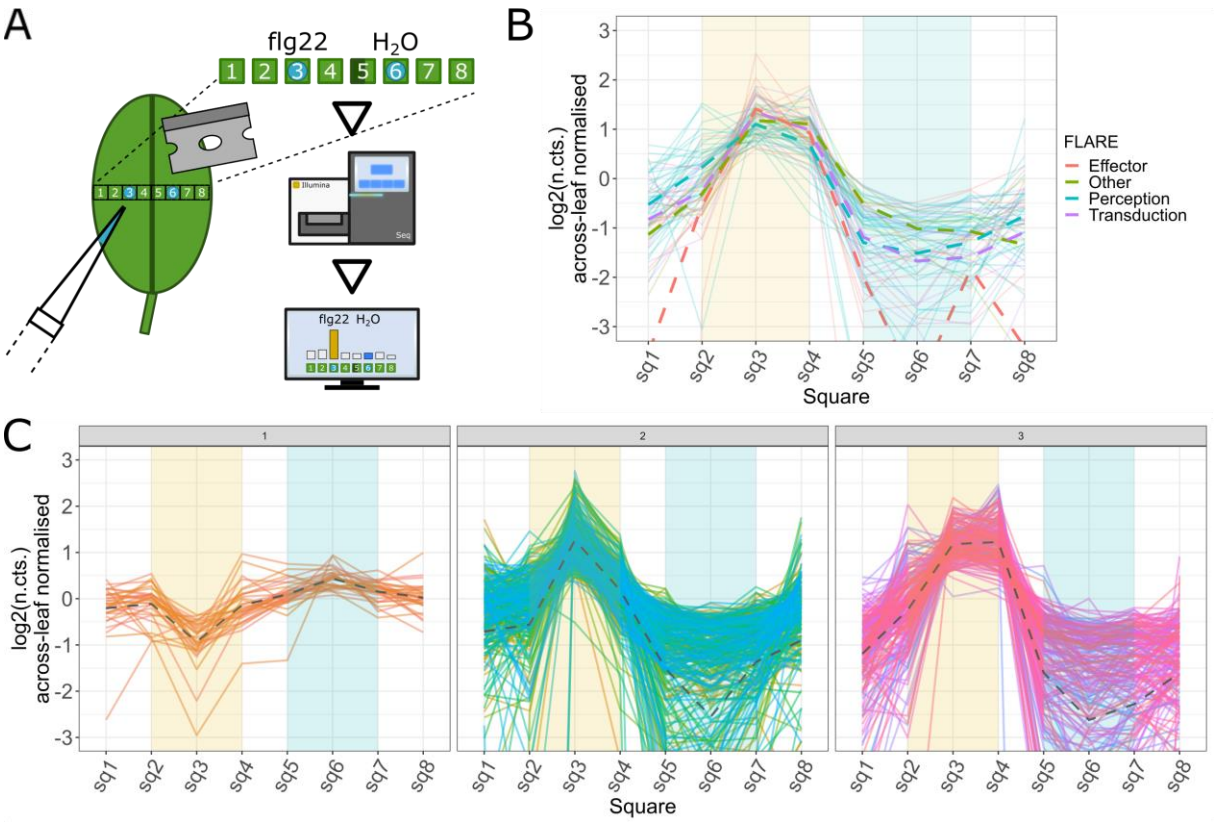

Figure 4 Elicitation of early *A. thaliana* defence response genes by droplet depositing the bacterial peptide flg22: (A) As a milder stress stimulus than flg22 syringe infiltration we pipetted a 1 µl droplet of 500 nM flg22 and, as an internal control, water on the abaxial surface of a leaf. 1 hour after droplet deposition we dissected a lateral section into 8 squares with square-1 and square-8 as leaf margins, square-3 as flg22 treated spot, square-6 as water treated spot and square-5 as midvein. Image (B) shows an overlay of the spatial expression patterns of the 63 FLARE genes characterised by Navarro et al. *[18]* present in our dataset. Each group is coloured separately, the average expression of each FLARE group is shown as the dashed line. Image (C) shows the spatial expression of all 523 detected DE genes grouped in three different clusters. From left to right: One cluster (1) contains genes which are lower expressed at the flg22 treatment area, two clusters contain genes with higher expression at the flg22 treatment spot in comparison to adjacent areas but with narrower (2) and broader (3) spatial expression. The yellow background in the plot indicates the flg22 treated area, the blue background indicates the water treated control area.

We analysed all clusters for enriched biological processes using GO-term analysis. We could not detect any enrichment in biological processes for the cluster containing the DE genes which were lower expressed at the flg22 site. The two clusters with expression peaks at the site of flg22 stimulation however enriched 135 and 122 biological processes. Of all biological processes 100 were shared between both clusters and 35 as well as 22 biological processes unique for each cluster

212 respectively (see: **Additional_file1.docx** and **Additional_file2.xlsx**). This suggests that biological
213 processes (host responses) could be associated with the spatial expression profiles of their
214 corresponding genes. To study this further we used the affinity propagation clustering algorithm [21]
215 to determine the number of clusters without a specified cluster number preference value. This
216 grouped the 523 DE genes into 36 more tightly resolved spatial expression clusters, comprising 35
217 clusters with between three and 57 genes and a single cluster containing only one gene (**Figure 5A**).
218 28 of 35 clusters were enriched for biological processes (see: **Additional_file3.csv**). To test if
219 different spatial expression patterns enrich different biological processes, we correlated all multi-
220 gene clusters based on the presence / absence of all enriched GO-terms. We saw little overlap in
221 biological processes between clusters, indicating that each spatial expression cluster enriched slightly
222 different GO-terms. (**Figure 5B** and **Additional_file3.csv**).

223

224 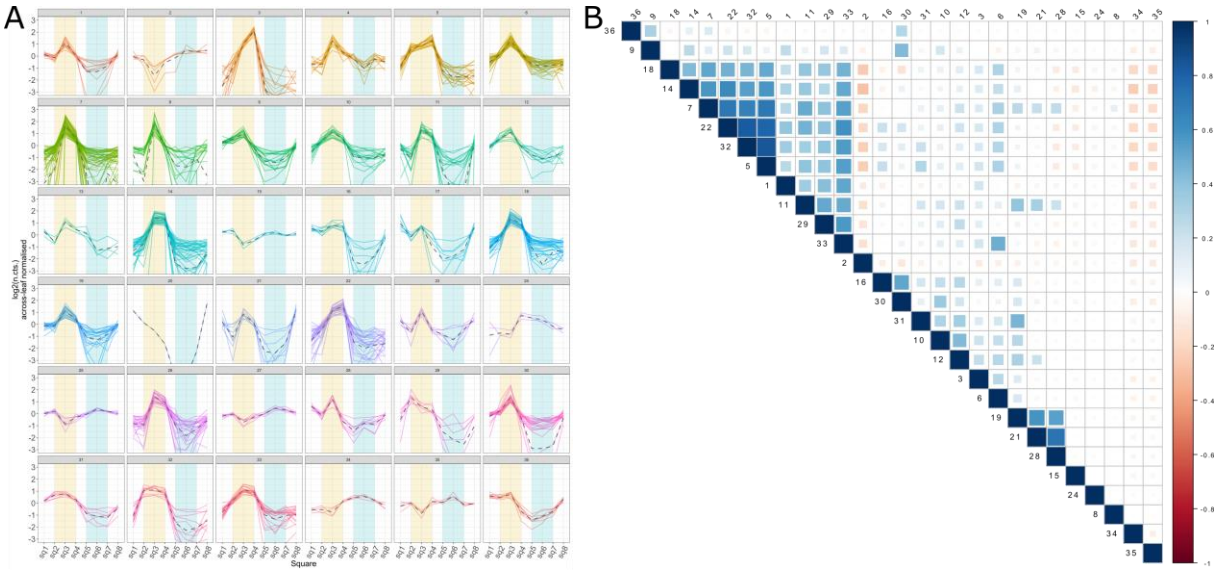

225 **Figure 5 Unsupervised clustering of flg22 elicited DE genes and GO-term correlation matrix of the predicted clusters:**
226 Figure (A) shows the expression profiles of the 523 flg22 elicited DE genes grouped to 36 clusters precisely clustered
227 according to their spatial expression pattern across the tested leaf area. Many of the clusters show differences in their
228 induction profile at the site of flg22 deposition (yellow background) but also differences in expression at the water treated
229 area (blue background) or the expression at the leaf boarders. Figure (B) shows the correlation analysis of the enriched GO-
230 terms from the genes of the spatial clusters shown in (A) – 28 clusters grouped with hierarchical clustering for enriched GO-
231 terms.

232 **Characterisation of spatial regulatory elements**

233 We characterised the expression patterns of the 36 obtained clusters in **Figure 5**. 11 clusters (1, 2, 6,
234 8, 12, 15, 23, 25, 28, 30, 35) showed a peak of higher expression at the site of flg22 perception. 14
235 clusters (3, 5, 7, 10, 11, 14, 18, 19, 21, 22, 26, 29, 32, 33) indicated spatially elevated gene expression
236 patterns with higher expression also at sites adjacent to the area of flg22 perception. The remaining
237 11 clusters showed less clear expression profiles (**Additional_file2.xlsx**).

238 To identify plant regulatory elements that are potentially involved in PAMP perception and signal
239 propagation to adjacent areas, we selected DE genes belonging to the flg22 locally and adjacently
240 elevated clusters, and then filtered the genes for the TAIR-10 [22] GO-terms 'receptor' and
241 'transcription'. This included the leucine-rich repeat receptor like kinase (LRR-RLK) *RLK7* (cluster 1)
242 which was locally elevated, whereas the LRR-RLK *CERK1* and the serine/threonine-protein kinase
243 *PSKR1* while strongly elevated at the area of flg22 perception were also broadly expressed
244 throughout all sites (cluster 7). We detected a larger set of 48 DE genes associated with
245 transcriptional processes. WRKY (15 genes), ERF (8 genes) and MYB (4 genes) transcription factor
246 family members [23–25] were the most abundant in our dataset.

247 To start to understand the possible gene regulatory network controlling this spatial expression we
248 used the TF2Network software [26] to search for putative regulatory interactions between these 48
249 DE genes i.e. by transcription factor binding. The resulting gene networks are built from genes with
250 at least one target and a q-value < 0.01 (see **Additional_file1.docx**). These linked 4 transcription
251 factors of which all belonged to the WRKY family (*WRKY11*, *WRKY15*, *WRKY17* and *WRKY47)* to 388
252 other DE genes indicating a possible regulatory network (TF2Network authors suggest their tools has
253 a very low false positive rate, whilst being sensitive enough to detect 75-92% of correct links).

254 Of the detected transcription factors *WRKY17* (cluster 4) and *WRKY47* (cluster 8) were associated
255 with local expression patterns, whereas *WRKY11* (cluster 10) and *WRKY15* (cluster 10) showed
256 spatially wider expression.

257 **Discussion**

258 The ability to profile gene expression patterns in small specific areas without bulk sequencing
259 provides access to lower level transcripts, especially tissue and cell specific ones [3–5,28–30]. Spatial,
260 low RNA-input transcriptomics methods allow deeper insights in how an organism develops and
261 reacts to its environment than conventional "gross-scale" RNA-seq methods [4–6]. By combining
262 rapid dissection with Grid-seq, we were able to reconstruct spatial transcriptional differences across
263 organs and localised defence responses.

264 Although some specialised protocols are already available to profile transcriptomes from minute
265 input amounts such as single-cells [2,10], or even nuclei [11,12], these detailed techniques do not
266 retain the spatial information of a starting tissue and any time-consuming experimental procedures
267 to preserve spatial data could induce experimental bias by altering the transcriptome. For spatial
268 analyses in plants LCM [14,15] methods for fine-scale transcriptome analyses are available, however,
269 these procedures are time-consuming and this limits the scale of the application. Large scale spatial
270 analysis have been performed in the past [8], but still required bulk sampling of material by pooling
271 multiple replicates. Methods relying on sample dissection and reaction-tube processing of tissue
272 sections to sequencing libraries have already proven to be able to identify transcripts patterns in the
273 zebrafish embryo [5] allowing to process multiple samples easily for modelling the transcriptome
274 landscape of an entire organism. Recently Giacomello et al. [6] published a workflow to blot the
275 transcriptome landscape from permeabilised plant tissues by vertical diffusion onto a slide
276 containing an array of barcoded primers and on slide library construction which maintained the
277 mRNA's location via the barcode. This method, for the first time in plants, allowed access to spatial
278 transcriptome data in thin tissue slices of plant organs with a great level of resolution. However,
279 gathering and optimisation of permeabilization conditions of thin tissue sections can be challenging
280 especially if the tissue due to the volume and shape of the sample, are not suitable to be processed
281 on an array and the workflow is only commercially accessible.

282 Plants grow in a microbiologically rich environment with their own microbiomes and even symbionts
283 [31], but they are also attacked by pathogens, pests, herbivores and other biotic stresses [32]. As
284 plants can't move away from attacks they defend themselves using molecular and cellular biology
285 responses, however overstimulation of these processes leads to stunted development and lower
286 fitness [17]. As plants must balance the need to defend themselves against constant plant-microbial
287 interactions and attack [17] we hypothesised that local attacks might be integrated into a plant-wide
288 defence response decision. Yet there are no appropriate assays to measure the molecular and cell
289 biology changes at the required resolution. Here, we demonstrate a novel micro-scale method to
290 pursue spatial transcriptomics experiments in plants in an easy manner based on easily accessible
291 methods in sequencing library construction and bioinformatics tools.

292 We developed a robust micro-spatial expression methodology that enables the creation of
293 transcriptome level maps from very small amounts of any eukaryotic tissue. The Grid-seq workflow
294 evolved by transferring elements from existing single-cell RNA-seq methods [33,34] from animal
295 systems to plants and refining these methods for stable, low-cost generation of sequencing libraries
296 from small amounts of RNA starting material. This allows the design of experiments in which spatial
297 information is required but only small pieces of tissue can be obtained. In the process of method
298 development, we tested and included several features to efficiently generate double stranded cDNA
299 (ds-cDNA) with reduced PCR amplification in both ds-cDNA synthesis and subsequent amplification
300 after Nextera tagmentation. We introduced sample specific barcodes in the Nextera amplification
301 step to allow pooling of 2304 of samples per sequencing run. This optimisation altogether allowed us
302 to construct sequencing libraries by hand for just £ 6.00 per library (see **Additional_file2.xlsx**) in
303 comparison to £ 65.56 for an Illumina TruSeq library (RS-122-2001, Illumina) or £ 62.60 for a
304 SMARTer PCR cDNA Synthesis Kit library (634926, TaKaRa).

305 In our benchmarking experiments we compared the Grid-seq workflow with the widely used Illumina
306 TruSeq sequencing protocol and show that the Grid-seq method compares well with this common
307 commercial RNA-seq protocol (see: **Additional_file1.docx**). We also show that Grid-seq can detect

308 transcript level differences across 1D leaf sections in distinct leaf elements such as leaf margins or
309 vascular tissues and that spatial mapping of transcript levels to specific sections of leaves is possible,
310 which allows drawing of transcriptional expression profiles across tissues. This easily used, low cost
311 protocol makes feasible experiments that require spatial transcriptome analysis.

312 To apply the Grid-seq method for studying biotic actions we challenged *A. thaliana* leaves with the
313 bacterial peptide flg22, a conserved 22 amino acid sequence of the bacteria flagellin protein, which
314 to the plant indicates an encounter with potentially pathogenic bacteria [35]. Plants recognize such
315 potential threats as the pathogenic cell surface molecules, so called Pathogen-Associated Molecular
316 Patterns (PAMPs), perceived by the plant Pattern Recognition Receptors (PRRs) on the plant cell
317 surface [36]. This event initiates an intracellular plant signalling cascade leading eventually to
318 immunity or disease [17,37]. In our experiments we could detect the triggering of immune and
319 defence response related biological processes and show that the results obtained by RNA-seq are
320 independently reproducible using qRT-PCR (see: **Additional_file1.docx**). We were able to find
321 overlap in our data with already described flg22 elicited (FLARE) genes from a gross-scale experiment
322 using a strong stimulus [18]. In comparative analyses of our dataset with the spatial expression
323 patterns of the described FLARE genes we were able to identify genes which share similar spatial
324 expression and are potential novel FLARE genes. Cluster based analysis of spatial expression data
325 revealed sets of genes with highly similar expression profiles enriched in distinct biological processes;
326 including FLARE genes to which we add new and increased expression resolution. Characterisation of
327 spatial cluster expression profiles highlighted plant regulatory elements with local or spatially
328 elevated expression levels and so potential short distance signal propagators upon flg22 stimulus.

329 In a proof of principle experiment applying of the oomycte *Albugo laibachii NC14* to *A. thaliana*
330 leaves we also recovered both host and pathogen transcript data, indicating that dual-host pathogen
331 experiments (between eukaryotic organisms) are possible (see: **Additional_file1.docx** and
332 **Additional_file2.xlsx**).

333 **Conclusions**

334 We find that Grid-seq allows reproducible spatial-transcriptome experiments in plant tissues. Proof
335 of concept experiments highlighted the usability of the method in characterising spatial differences
336 within organs, and changes induced by biotic stimuli of bacterial PAMPs. The workflow also
337 compares well to widely used RNA-seq protocols such as Illumina TruSeq sequencing but can be
338 conducted at a fraction (~ 1/10th) of the library preparation costs of Illumina TruSeq. Furthermore,
339 as our ds-cDNA synthesis method is based on single-cell technologies [33], even smaller sections
340 could be processed while maintaining efficient library and sequencing results.

341 **Methods**

342 **Plant growth**

343 For our experiments we used 4 – 6 week old *A. thaliana* Col-0 plants that were grown in a controlled
344 environment room with an 8 hours light, 16 hour dark cycle at a constant temperature of 22 °C and
345 70 % humidity.

346 **Flg22 exposure experiments**

347 Before flg22 treatment experiments, we transferred the plants from the controlled environment
348 room to a laboratory working bench (room with constant light exposure and temperature). To elicit
349 plant responses with flg22 we either syringe infiltrated [38] the peptide or spotted a droplet of flg22
350 on a leaf using a pipette.

351 To produce small, local infiltration spots we used a 1 ml syringe (BS01T, R&L Slaughter Ltd, Basildon,
352 UK) loaded with 500 nM flg22 peptide solution. By application of mild pressure on the plunger of the
353 syringe when infiltrating we produced an approximately 2 - 3 mm diameter infiltration spot on the
354 left-hand side of a leaf. In parallel to flg22 infiltration we produced an infiltration series with
355 DNase/RNase-free water as control. The plants were subsequently incubated on the laboratory
356 working bench for 1 hour until sampling.

357 For the flg22 spotting experiment we loaded a 1 µl droplet of 500 nM flg22 on the abaxial surface of
358 a leaf using a pipette (diameter approximately 1 mm). The flg22 was pipetted onto the left half of the
359 leaf and a 1 µl droplet of the water control droplet spotted on the right half of the leaf. After spotting
360 the plants were incubated for 1 hour on the laboratory bench before sampling.

361 **Leaf sectioning and sample harvesting**

362 We used single margin razor blades (T586, Agar Scientific Ltd., Stansted, UK) to cut leaves into
363 approximately 1 mm^2 small leaf squares. To create a clean surface for cutting we used the pealed,
364 non-sticky paper cover of a 96-well plate seal (AB0580, Thermo Fisher Scientific, Waltham, USA).
365 With a previously in RNaseZAP (AM9780, Thermo Fisher Scientific, Waltham, USA) washed and air-
366 dried forceps (T083, TAAB Laboratories Equipment Ltd, Berks, UK) we transferred each leaf square
367 immediately after cutting into a well of a 96-well plate (E1403-0100-C, Starlab, Milton Keynes, UK)
368 which we had pre-cooled on a 96-well metal block in dry ice (- 70 ^{o}C), or alternatively, a dry-ice
369 cooled 1.5 ml tube (10051232, Fisher Scientific, Loughborough, UK). The sample wells of 96-well
370 plates were sealed using domed PCR cap strips (AB0602, Thermo Fisher Scientific, Waltham, USA).
371 Post harvesting the samples were stored at -80 ^{o}C until use.

372 **Leaf sample lysis and preparation for mRNA extraction**

373 To lyse the leaf samples stored in 1.5 ml tubes we first added 10 µl lysis buffer composed of 100 mM
374 Tris-HCl pH 7.5 (BP1757, Fisher Scientific, Loughborough, UK), 500 mM LiCl (L7026, Sigma Aldrich, St.
375 Louis, USA), 10 mM EDTA pH 8.0 (E7889, Sigma Aldrich, St. Louis, USA), 1% LiDS (L4632, Sigma
376 Aldrich, St. Louis, USA), 5 mM DTT (18064014, Thermo Fisher Scientific, Waltham, USA) to each
377 sample immediately after removing the sample tube from the cold storage.

378 We subsequently ground the leaf sections in lysis buffer using polypropylene pestles (Z359947, Sigma
379 Aldrich, St. Louis, USA), which, before use, were washed with RNaseZAP (R2020, Sigma Aldrich, St.
380 Louis, USA, three times with 80% ethanol (32221, Sigma Aldrich, St. Louis, USA) rinsed with UltraPure
381 DNase/RNase-Free Distilled Water (10977049, Thermo Fisher Scientific, Waltham, USA) and air-dried

382 after washing. After sample lysis we transferred the lysate to an ice-cooled 96-well plate and
383 continued with the mRNA extraction.

384 Samples stored in 96-well plates were lysed by using 1 mm diameter grade 1000 hardened 1010
385 carbon steel ball bearings (Simply Bearings Ltd, Leigh, UK). For this, before use of the ball bearings,
386 we treated a bulk batch sequentially with RNaseZAP and DNA AWAY, after this washed the ball
387 bearings three times with 80% ethanol and transferred them to sterile screw-cap 2.0 ml tubes
388 (E1420-2341, Starlab, Milton Keynes, UK) and heat dried with a slightly loosened lid on a 95 ^{o}C
389 heating block (N2400-4001, Starlab, Milton Keynes, UK).

390 To lyse the collected leaf samples stored in a 96-well plate, we transferred the 96-well plate to a dry
391 ice temperature cooled 96-well metal block. We carefully opened the domed PCR cap lids to avoid
392 sample spillage and added the 4 – 6 (room temperature) ball bearings to each sample well. After this
393 we transferred 10 µl lysis buffer to each well and re-sealed the plate with new domed PCR cap lids,
394 and immediately proceeded to the 2010 Geno/Grinder (SPEX SamplePrep, Stanmore, UK) disrupting
395 the samples for 30 seconds at 1750 rpm. We gathered the sampled using a centrifuge (Centrifuge
396 5910 R, Eppendorf UK Ltd, Stevenage, UK) for 10 seconds at 2000 x rcf. A strongly green-coloured
397 solution without any remaining solid leaf material indicated good sample lysis. If satisfactory sample
398 lysis was not achieved, we disrupted the samples again for another 10 seconds on the 2010
399 Geno/Grinder at 1750 rpm and centrifuged for 30 seconds at 2000 x rcf. We immediately transferred
400 the lysis solutions into a new 96-well plate using a 10 µl multichannel pipette. After transfer of the
401 lysis solutions, we stored the new 96-well plate on ice, discarded the 96-well plate containing the ball
402 bearings and proceeded immediately with mRNA extraction. For a laboratory compatible version of
403 the workflow see: **Additional_file1.docx**.

404 **Leaf mRNA purification**

405 The leaf tissue mRNA was purified using 1 µl NEBNext Poly(A) mRNA Magnetic Isolation Module
406 oligo-dT(25) beads (E7490, New England Biolabs Ltd, Hitchin, UK) per extraction. Previous to the

407 extraction the required volume of oligo-dT(25) magnetic beads was washed twice in 200 µl lysis
408 buffer on a DynaMag-2 Magnet rack (12321D, Thermo Fisher Scientific, Waltham, USA) and
409 resuspended in 10 µl lysis buffer for each 1 µl oligo-dT(25) beads input volume. The beads were
410 mixed by a quick vortex and 10 µl of the resuspended beads were transferred to each well of the 96-
411 well plate containing the lysis solutions. The wells were sealed with domed PCR cap strips, the 96-
412 well plate vortexed briefly and attached to a tube rotator (444-0502, VWR International Ltd,
413 Luterworth, UK) with adhesive tape. After 10 minutes rotation we collected the lysis solution at the
414 bottom of the wells by spinning the plate for 10 seconds at 2000 x rcf and pelleted the oligo-dT(25)
415 magnetic beads on a 96-ring magnetic plate (A001219, Alpaqua, Beverly, USA). Using a multichannel
416 pipette we washed the oligo-dT(25) magnetic beads twice with 50 µl Wash Buffer A (10mM Tris-HCl
417 pH7.5, 0.15M LiCl, 1mM EDTA, 0.1% LiDS) and once with Wash Buffer B (10mM Tris-HCl pH 7.5,
418 0.15M LiCl, 1mM EDTA). After washing we centrifuged the plate for 10 seconds at 2000 x rcf to
419 collect the remaining Wash Buffer B at the bottom of the tube, pelleted the oligo-dT(25) magnetic
420 beads on a magnet and removed the remaining volume of Wash Buffer B with a multichannel
421 pipette. The oligo-dT(25) beads were resuspended immediately in 8 µl DNase/RNase-Free water,
422 incubated for 2 minutes at 80 ^{o}C on a G-Storm GS1 thermal cycler (G-Storm, Somerton, UK), then
423 immediately pelleted on a 96-ring magnetic plate to elute the mRNA off and separate from the oligo-
424 dT(25) beads. The solutions containing the purified mRNA were immediately transferred to a new 96-
425 well plate, which was placed in a - 80 ^{o}C freezer until needed. For a laboratory compatible version of
426 the workflow see: **Additional_file1.docx**.

427 **Double-stranded cDNA synthesis reaction**

428 For ds-cDNA synthesis we used a protocol based on the template switching mechanism of the
429 reverse transcriptase enzymes [39]. Briefly: 2.50 µl extracted mRNA was mixed with 2 µl 5x First
430 Strand buffer (18064014, Thermo Fisher Scientific, Waltham, USA), 1 µl 10 mM dNTPs (10297018,
431 Thermo Fisher Scientific, Waltham, USA), 1 µl 5'-biotinylated 10 µM STRT-V3-T30-VN oligonucleotide:
432 5'-/5Biosg/TTAAGCAGTGGTATCAACGCAGAGTCGACTTTTTTTTTTTTTTTTTTTTTTTTTTTTTVN-3'

433 (Integrated DNA Technologies, Leuven, BE), 1 µl 20 mM DTT (18064014, Thermo Fisher Scientific,
434 Waltham, USA), 0.10 µl 40 U/µl RNase Inhibitor (M0314S, New England Biolabs Ltd, Hitchin, UK), 0.25
435 µl 10 µM template switching oligo 5'-
436 AAGCAGTGGTATCAACGCAGAGTGCAGUGCUTGATGATGGrGrGrG-3' (Integrated DNA Technologies,
437 Leuven, BE), 0.30 µl 200 U/µl SuperScript II Reverse Transcriptase (18064014, Thermo Fisher
438 Scientific, Waltham, USA), 0.30 µl 100 µM $MnCl_2$ (M1787, Sigma Aldrich, St. Louis, USA) and 1.55 µl
439 DNase/RNase-Free water to a total reaction volume of 10 µl. The reverse transcription reaction was
440 run in a G-Storm GS1 thermal cycler for 90 minutes at 42 ^{o}C with additional 10 minutes at 72 ^{o}C to
441 inactivate the reverse transcriptase. After reverse transcription we immediately added 2 µl RNase H
442 (M0297S, New England Biolabs Ltd, Hitchin, UK) diluted to 0.5 U/µl (5 U/µl stock concentration) to
443 the reaction and incubated the reaction in the GS1 thermal cycler for 30 minutes at 37 ^{o}C. The RNase
444 H treated reactions were purified using a 0.83x (10 µl) AMPure XP bead ratio (Beckman Coulter, High
445 Wycombe, UK) and eluted in 18 µl 1x TE buffer. After this step we added 5 µl 5x Kapa HiFi PCR buffer
446 (KK2102, KAPA BioSystems, Wilmington, USA), 0.75 µl 10 mM dNTPs, 0.75 µl 10 µM PCR+G primer 5'-
447 GAAGCAGTGGTATCAACGCAGAGT-3' (Integrated DNA Technologies, Leuven, BE) and 0.50 µl 1 U/µl
448 Kapa HiFi polymerase (KK2102, KAPA BioSystems, Wilmington, USA) to the cleaned ds-cDNA resulting
449 in a total reaction volume of 25 µl and amplified the ds-cDNA in a G-Storm GS1 thermal cycler
450 according to the following programme: (1) 3 minutes at 94 ^{o}C, (2) 17 cycles with 30 seconds at 94 ^{o}C,
451 30 seconds at 63 ^{o}C and 1 minute 30 seconds at 72 ^{o}C, (3) a final elongation step for 5 minutes at 72
452 ^{o}C. The amplified libraries were purified using a 1x (25 µl) AMPure XP bead ratio and eluted in 20 µl
453 1x TE buffer. The ds-cDNA libraries could be stored at this point in a -20 ^{o}C freezer. Before continuing
454 with Illumina sequencing library preparation, we measured the ds-cDNA library concentrations with
455 the Qubit 2.0 Fluorometer (Thermo Fisher Scientific, Waltham, USA) dsDNA HS Assay Kit reagents
456 (Q32854, Thermo Fisher Scientific, Waltham, USA) and also assessed the size distributions of
457 randomly picked libraries on an Agilent Bioanalyser (G2939BA, Agilent Technologies, Stockport, UK)
458 using the Agilent High Sensitivity DNA Kit (5067-4626, Agilent Technologies, Stockport, UK).

459 At later stages we modified the ds-cDNA synthesis integrating elements of the Smart-seq2 protocol
460 [40]. The reverse transcription reactions of Grid-seq-1.0 (as described above) and Smart-seq2 were
461 already highly similar, but Smart-seq2 had proven to require less hands-on time than the Grid-seq-
462 1.0 reverse transcription workflow. Grid-seq-1.1 uses the Smart-seq2 ds-cDNA synthesis with minor
463 modifications, briefly: 2.50 µl extracted mRNA were combined with 1 µl 10 µM Smart-seq2 Oligo-
464 dT30VN (5'-AAGCAGTGGTATCAACGCAGAGTACTTTTTTTTTTTTTTTTTTTTTTTTTTTTTTVN-3', Integrated
465 DNA Technologies, Leuven, BE) and 1 µl 10 mM dNTPS to a total volume of 4.5 µl. To anneal the
466 Smart-seq2 Oligo-dT30VN we incubated the library for 30 seconds at 72 ^{o}C and snap-cooled the
467 mixture on ice. The reverse transcription was conducted by adding the following reagents to the
468 reaction with a final reaction volume of 10 µl: 2 µl 5x First Strand buffer, 2 µl 5 M betaine (B0300,
469 Sigma Aldrich, St. Louis, USA), 1 µl 1 M $MgCl_2$ (AM9530G, Thermo Fisher Scientific, Waltham, USA),
470 0.5 µl 100 mM DTT, 0.25 µl 40 U/µl RNase Inhibitor (2313A, Takara Clontech, Mountain View, USA),
471 0.10 µl 10 µM Smart-seq2 template switching oligo (5'-AAGCAGTGGTATCAACGCAGAGTACATrGrG+G-
472 3', Exiqon, Vedbaek, DK), 0.50 µl 200 U/µl SuperScript II Reverse Transcriptase, and 0.09 µl
473 DNase/RNase-free water. We performed the reverse transcription reaction for (1) 90 minutes at 42
474 ^{o}C, (2) 15 cycles with 2 minutes at 50 ^{o}C and 2 minutes at 42 ^{o}C and finally (3) 15 minutes at 70 ^{o}C.
475 After reverse transcription we added 12.50 µl 2x Kapa HiFi HotStart ReadyMix (KK2601, KAPA
476 BioSystems, Wilmington, USA), 0.25 µl 10 µM Smart-seq2 IS-PCR primers (Integrated DNA
477 Technologies, Leuven, BE) and 2.25 µl DNase/RNase-Free water to the reaction resulting in a total
478 volume of 15 µl per reaction. Amplification was performed in a G-Storm GS1 cycler according to the
479 programme: (1) 3 minutes at 98 ^{o}C, (2) 15 cycles with 20 seconds at 98 ^{o}C, 15 seconds at 67 ^{o}C and 6
480 minutes at 72 ^{o}C and a (3) final elongation step for 5 minutes at 72 ^{o}C. The PCR reactions were
481 purified using a 0.65 x (9.75 µl) AMPure XP cleanup and eluted in 20 µl 1 x TE buffer. After cleanup
482 we measured the ds-cDNA library concentrations with the Qubit 2.0 Fluorometer dsDNA HS Assay Kit
483 reagents and loaded randomly selected libraries on the Agilent Bioanalyser using the Agilent High

484 Sensitivity DNA Kit before continuing with Illumina sequencing library prepration. For a laboratory
485 compatible version of the workflow see: **Additional_file1.docx**.

486 **Illumina library preparation from ds-cDNA**

487 We prepared Illumina sequencing libraries using an Illumina Nextera (FC-121-1030, Illumina
488 Cambridge, UK) based protocol with minor modifications: we exclusively used the Tagment DNA
489 Enzyme 1 and the Tagment DNA Buffer and amplified the tagmented DNA with the Kapa 2G Robust
490 Polymerase (KK5024, Sigma Aldrich, St. Louis, USA). We used custom Nextera barcodes that allow us
491 to multiplex hundreds of samples (see: **Additional_file2.xlsx**) [41].

492 We reduced the costs of the library preparation by reducing the total tagmentation reaction volume
493 to 5 µl (from 50 µl as recommended) with 1 ng ds-cDNA library input and using less enzyme. We
494 performed a titration experiment of Tagment DNA Enyzme vs. 1 ng of selected ds-cDNA libraries
495 aiming for Illumina sequencing libraries with a modal insert size distribution in the range of 400-500
496 bp with little short insert fragments and found that 0.1 µl Nextera enzyme was optimal.

497 The Nextera reactions were performed by combining 1 ng of ds-cDNA (air-dried over-night at room
498 temperature in a drawer with the 96-well plate loosely covered to allow evaporation of liquid) with
499 2.5 µl 2 x Nextera buffer, 2.4 µl water and 0.1 µl Nextera enzyme on ice. The tagmentation plate was
500 immediately transferred for 5 minutes at 55 ^{o}C on a G-Storm GS1 thermal cycler. Meanwhile we
501 prepared a fresh 96-well plate with 2.0 µl 2.5 µM P5 and 2.0 µl 2.5 µM P7 custom multiplexing
502 primers (see: **Additional_file2.xlsx**). After tagmentation we transferred the tagmentation reactions
503 to the previously prepared 96-well plate containing the sequencing adapters (see above) and added
504 the following to each well: 5.00 µl 5 x Kapa 2G Robust Buffer, 0.50 µl 10 mM dNTPs, 0.10 µl 5 U / µl
505 Kapa 2G Robust Polymerase, 10.4 µl water to a total final volume of 25 µl.

506 Amplification was performed on a GStorm GS-1 cycler using the following program: (1) 3 minutes at
507 72 ^{o}C, 1 minute at 95 ^{o}C (2) 11 cycles of 10 seconds at 95 ^{o}C, 30 seconds at 65 ^{o}C, 2 minutes 30
508 seconds at 72 ^{o}C (2) a final elongation step for 2 minutes 30 seconds at 72°C. After amplification we

509 purified the libraries using a 0.64x ratio (16 µl) AMPure XP beads, measured the library yields with
510 the Qubit 2.0 Fluorometer dsDNA HS Assay Kit reagents and assessed the size distributions of
511 randomly selected libraries on the Agilent Bioanalyser with the Agilent High Sensitivity DNA Kit. For a
512 laboratory compatible version of the workflow see: **Additional_file1.docx**.

513 **Sample pooling and sequencing**

514 For sequencing all library concentrations were determined using Qubit 2.0 Fluorometer using the
515 dsDHA HS Assay kit reagents and pooled at equal molarity. The profile and concentration of the final
516 library pool was assessed on the Agilent Bioanalyser using Agilent High Sensitivity DNA Kit
517 Sequencing reagents. After this the pooled samples were shipped to the Earlham Institute for
518 sequencing. Quality control and data demultiplexing was performed by the Earlham Institute
519 Genomics Pipelines facilities. Samples were sequenced using Illumina HiSeq2500 50 base single-end
520 rapid run sequencing for the *A. thaliana* wounding and *A. thaliana* flg22 infiltration datasets Illumina
521 NextSeq500 75 base single-end for the *A. thaliana* untreated leaf dataset and Illumina HiSeq4000 150
522 base paired-end sequencing for the *A. thaliana* flg22 droplet spotting experiment.

523 **Data quality control and mapping**

524 The sequencing reads were quality controlled using FastQC-0.11.5 [42]. After quality control we used
525 cutadapt-1.17 [43] to trim low-quality bases (-q 20) and remove Oligo-dT, template switching oligos,
526 primer and Illumina Nextera library preparation sequences (-n 5 -e 0.05 –overlap 10). We also
527 removed sequences with less than 40 bases (--minimum-length 40) and sequences containing N's (--
528 max-n 0) from the dataset with cutadapt-1.17. After adapter and quality trimming we re-assessed
529 the reads a second time with FastQC-0.11.5. We mapped the reads to the *A. thaliana* TAIR10 release
530 37 genome assembly using STAR-2.5.1b [44] default settings and assessed mapping scores,
531 duplication levels, GC-bias and gene-body coverage after mapping with RSeQC-2.6.4 [45]. Reads were
532 counted with HTSeq-count-0.6.0 [46] default settings.

533 **Differential-expression analysis, GO-term enrichment and plant metabolic pathway enrichment**

534 Differential expression analysis was performed using DESEq2-1.20.0 [47] in the statistical language R-
535 3.5.1 using the workflow described by Love et al. [48] but by pre-filtering the dataset for rows with
536 less than 10 rather than 1 raw read counts. DE-genes were called with a q-value threshold < 0.05%.

537 Across leaf DE-gene expression plots were prepared using R-3.5.1; in brief: We imported all samples
538 with DESeq2-1.20.0 and calculated a table with normalised expression values as in the workflow
539 described by Love et al. [48]. Next, we calculated the average expression value of each gene in each
540 leaf square across all biological replicates. As a final step we normalised the expression values of the
541 leaf squares. For this we divided the mean expression value of each leaf square of a gene with the
542 mean expression value across all leaf squares of the same gene. The log2 transformed plots of the so
543 normalised data were generated using ggplot2-3.1.0 [49]. Affinity propagation clustering of the
544 normalised expression tables was performed using the R-3.5.1 library apcluster-1.4.7 and a Pearson
545 distance matrix of the normalised data for apclustK and apclust [21] default settings. The number of
546 clusters was either empirically determined by continuously increasing the preferred cluster number
547 in the apclustK function and visualising the expression profiles of the clusters using ggplot2-3.1.0 or
548 determined without providing a cluster number preference value using the apclust function.

549 GO-term enrichment analysis on DE-genes was performed using the R-3.5.1 Bioconductor library
550 ClusterProfiler-3.8.1 [50] with the settings (Statistical test: Hypergeometric test, Multiple testing
551 correction: Benjamini & Hochberg False Discovery Rate correction, False Discovery Rate cutoff: 0.01)
552 and the Bioconductor library org.At.tair.db-3.6.0 as organism database [51].

553 **Additional files**

554 **Additional_file1.docx:** Comparison of Grid-seq with Illumina TruSeq, qRT-PCR validation of DE gene
555 expression, wounding time-series GO enrichment, *Albugo laibachii* spatial transcriptomics
556 experiment, all wet-lab protocols of the Grid-seq workflow.

557 **Additional_file2.xlsx:** Read numbers, ENA accessions, DE genes, GO accessions, clustering
558 information, FLARE associations of experiments.

559 **Additional_file3.xlsx:** GO-term enrichments of spatial affinity propagation clustering.

560 **Ethics approval and consent to participate**

561 Not applicable.

562 **Consent for publication**

563 This study abides by UK guidelines and legislation for plant science research.

564

565 **Availability of data and material**

566 Sequencing reads for the Grid-seq vs. TruSeq comparison are available under the ENA study
567 accession number PRJEB31337. Sequencing reads for the wounding experiment are available under
568 the ENA study accession number PRJEB31311. Sequencing reads for the untreated leaf spatial
569 transcriptomics experiment are available under the ENA study accession number PRJEB31314.
570 Sequencing reads for the flg22 / water infiltration experiment are available under the ENA study
571 accession number PRJEB31312. Sequencing reads for the flg22 / water droplet spotting experiment
572 are available under the ENA study accession number PRJEB31313. Sequencing reads for the *Albugo*
573 *laibachii* x *Arabidopsis.thaliana* spatial transcriptomics experiment are available under the ENA study
574 accession number PRJEB31803.

575 **Competing Interests**

576 The authors declare no competing interests.

577 **Funding**

578 This work was strategically funded by the Biotechnology and Biological Sciences Research Council
579 (BBSRC), Institute Strategic Programme Grant (BB/J004669/1) at the Earlham Institute (formerly The
580 Genome Analysis Centre, Norwich), a BBSRC National Capability Grant (BB/J010375/1), a BBSRC Core

581 Strategic Programme Grant (BB/CSP17270/1), a BBSRC DTP Studentship Award (BB/M011216/1) and
582 by the Natural History Museum.

583 **Authors' contributions**

584 M.G., W.V. and D.H. established protocols. M.G., W.V. and A.L. prepared sequencing libraries. M.G.
585 analysed the data. I.M. advised on protocols and data analysis. M.G. and M.D.C. wrote the
586 manuscript. W.V., M.G. and M.D.C. designed the study.

587 **Acknowledgements**

588 We thank David Prince for providing the *A. laibachii* NC14.

589 **References**

590 1. Müller B, Grossniklaus U. Model organisms — A historical perspective. J Proteomics.
591 2010;73:2054–63.

592 2. Mincarelli L, Lister A, Lipscombe J, Macaulay IC. Defining Cell Identity with Single-Cell Omics.
593 PROTEOMICS. 2018;1700312.

594 3. Crosetto N, Bienko M, van Oudenaarden A. Spatially resolved transcriptomics and beyond. Nat Rev
595 Genet. 2015;16:57–66.

596 4. Stahl PL, Salmen F, Vickovic S, Lundmark A, Navarro JF, Magnusson J, et al. Visualization and
597 analysis of gene expression in tissue sections by spatial transcriptomics. Science. 2016;353:78–82.

598 5. Junker JP, Noël ES, Guryev V, Peterson KA, Shah G, Huisken J, et al. Genome-wide RNA
599 Tomography in the Zebrafish Embryo. Cell. 2014;159:662–75.

600 6. Giacomello S, Salmén F, Terebieniec BK, Vickovic S, Navarro JF, Alexeyenko A, et al. Spatially
601 resolved transcriptome profiling in model plant species. Nat Plants. 2017;3:17061.

602 7. Rusk N. Genomics: Spatial transcriptomics. Nat Methods. 2016;13:710–1.

603 8. Mulema JMK, Denby KJ. Spatial and temporal transcriptomic analysis of the Arabidopsis thaliana-
604 Botrytis cinerea interaction. Mol Biol Rep. 2012;39:4039–49.

605 9. Ghawana S, Paul A, Kumar H, Kumar A, Singh H, Bhardwaj PK, et al. An RNA isolation system for
606 plant tissues rich in secondary metabolites. BMC Res Notes. 2011;4:85.

607 10. Borges F, Gardner R, Lopes T, Calarco JP, Boavida LC, Slotkin R, et al. FACS-based purification of
608 Arabidopsis microspores, sperm cells and vegetative nuclei. Plant Methods. 2012;8:44.

609 11. Deal RB, Henikoff S. The INTACT method for cell type–specific gene expression and chromatin
610 profiling in Arabidopsis thaliana. Nat Protoc. 2010;6:56.

611 12. Gaiero P, Šimková H, Vrána J, Santiñaque FF, López-Carro B, Folle GA, et al. Intact DNA purified
612 from flow-sorted nuclei unlocks the potential of next-generation genome mapping and assembly in
613 Solanum species. MethodsX. 2018;5:328–36.

614 13. Duncan S, Olsson T, Hartley M, Dean C, Rosa S. Single Molecule RNA FISH in Arabidopsis Root
615 Cells. BIO-Protoc [Internet]. 2017 [cited 2018 Jul 5];7. Available from: https://bio-protocol.org/e2240

616 14. Kerk NM. Laser Capture Microdissection of Cells from Plant Tissues. PLANT Physiol. 2003;132:27–
617 35.

618 15. Chan AC, Khan D, Girard IJ, Becker MG, Millar JL, Sytnik D, et al. Tissue-specific laser
619 microdissection of the *Brassica napus* funiculus improves gene discovery and spatial identification of
620 biological processes. J Exp Bot. 2016;67:3561–71.

621 16. Martin LBB, Nicolas P, Matas AJ, Shinozaki Y, Catalá C, Rose JKC. Laser microdissection of tomato
622 fruit cell and tissue types for transcriptome profiling. Nat Protoc. 2016;11:2376–88.

623 17. Jones JDG, Dangl JL. The plant immune system. Nature. 2006;444:323–9.

624 18. Navarro L. The Transcriptional Innate Immune Response to flg22. Interplay and Overlap with Avr
625 Gene-Dependent Defense Responses and Bacterial Pathogenesis. PLANT Physiol. 2004;135:1113–28.

626 19. Farmer E, Farmer E, Mousavi S, Lenglet A. Leaf numbering for experiments on long distance
627 signalling in Arabidopsis. Protoc Exch [Internet]. 2013 [cited 2016 Nov 3]; Available from:
628 http://www.nature.com/protocolexchange/protocols/2787

629 20. Supek F, Bošnjak M, Škunca N, Šmuc T. REVIGO Summarizes and Visualizes Long Lists of Gene
630 Ontology Terms. Gibas C, editor. PLoS ONE. 2011;6:e21800.

631 21. Frey BJ, Dueck D. Clustering by Passing Messages Between Data Points. Science. 2007;315:972–6.

632 22. Berardini TZ, Reiser L, Li D, Mezheritsky Y, Muller R, Strait E, et al. The arabidopsis information
633 resource: Making and mining the "gold standard" annotated reference plant genome: Tair: Making
634 and Mining the "Gold Standard" Plant Genome. genesis. 2015;53:474–85.

635 23. Pandey SP, Somssich IE. The Role of WRKY Transcription Factors in Plant Immunity. PLANT
636 Physiol. 2009;150:1648–55.

637 24. Xie Z, Nolan TM, Jiang H, Yin Y. AP2/ERF Transcription Factor Regulatory Networks in Hormone
638 and Abiotic Stress Responses in Arabidopsis. Front Plant Sci. 2019;10:228.

639 25. Dubos C, Stracke R, Grotewold E, Weisshaar B, Martin C, Lepiniec L. MYB transcription factors in
640 Arabidopsis. Trends Plant Sci. 2010;15:573–81.

641 26. Kulkarni SR, Vaneechoutte D, Van de Velde J, Vandepoele K. TF2Network: predicting transcription
642 factor regulators and gene regulatory networks in Arabidopsis using publicly available binding site
643 information. Nucleic Acids Res. 2018;46:e31–e31.

644 27. Iwata Y, Fedoroff NV, Koizumi N. *Arabidopsis* bZIP60 Is a Proteolysis-Activated Transcription
645 Factor Involved in the Endoplasmic Reticulum Stress Response. Plant Cell. 2008;20:3107–21.

646 28. Ryu KH, Huang L, Kang HM, Schiefelbein J. Single-Cell RNA Sequencing Resolves Molecular
647 Relationships Among Individual Plant Cells. Plant Physiol. 2019;179:1444–56.

648 29. Denyer T, Ma X, Klesen S, Scacchi E, Nieselt K, Timmermans MCP. Spatiotemporal Developmental
649 Trajectories in the Arabidopsis Root Revealed Using High-Throughput Single-Cell RNA Sequencing.
650 Dev Cell. 2019;48:840-852.e5.

651 30. Jean-Baptiste K, McFaline-Figueroa JL, Alexandre CM, Dorrity MW, Saunders L, Bubb KL, et al.
652 Dynamics of gene expression in single root cells of A. thaliana. Plant Cell. 2019;tpc.00785.2018.

653 31. Karasov TL, Almario J, Friedemann C, Ding W, Giolai M, Heavens D, et al. Arabidopsis thaliana and
654 Pseudomonas Pathogens Exhibit Stable Associations over Evolutionary Timescales. Cell Host Microbe.
655 2018;24:168-179.e4.

656 32. Dangl JL, Horvath DM, Staskawicz BJ. Pivoting the Plant Immune System from Dissection to
657 Deployment. Science. 2013;341:746–51.

658 33. Picelli S, Faridani OR, Björklund ÅK, Winberg G, Sagasser S, Sandberg R. Full-length RNA-seq from
659 single cells using Smart-seq2. Nat Protoc. 2014;9:171–81.

660 34. Macaulay IC, Haerty W, Kumar P, Li YI, Hu TX, Teng MJ, et al. G&T-seq: parallel sequencing of
661 single-cell genomes and transcriptomes. Nat Methods. 2015;12:519–22.

662 35. Denoux C, Galletti R, Mammarella N, Gopalan S, Werck D, De Lorenzo G, et al. Activation of
663 Defense Response Pathways by OGs and Flg22 Elicitors in Arabidopsis Seedlings. Mol Plant.
664 2008;1:423–45.

665 36. Zipfel C. Pattern-recognition receptors in plant innate immunity. Curr Opin Immunol. 2008;20:10–
666 6.

667 37. Bent A. Resistance from relatives. Nat Biotechnol. 2016;34:620–621.

668 38. Underwood W, Somerville SC. Perception of conserved pathogen elicitors at the plasma
669 membrane leads to relocalization of the Arabidopsis PEN3 transporter. Proc Natl Acad Sci.
670 2013;110:12492–7.

671 39. Zhu YY, Machleder EM, Chenchik A, Li R, Siebert PD. Reverse transcriptase template switching: a
672 SMART approach for full-length cDNA library construction. BioTechniques. 2001;30:892–7.

673 40. Picelli S, Björklund \AAsa K., Faridani OR, Sagasser S, Winberg G, Sandberg R. Smart-seq2 for
674 sensitive full-length transcriptome profiling in single cells. Nat Methods [Internet]. 2013 [cited 2015
675 Jan 6]; Available from: http://www.nature.com/nmeth/journal/vaop/ncurrent/full/nmeth.2639.html

676 41. Beier S, Himmelbach A, Colmsee C, Zhang X-Q, Barrero RA, Zhang Q, et al. Construction of a map-
677 based reference genome sequence for barley, Hordeum vulgare L. Sci Data. 2017;4:170044.

678 42. FastQC: a quality control tool for high throughput sequence data. 2010.
679 http://www.bioinformatics.babraham.ac.uk/projects/fastqc. Accessed 31 Jan 2017.

680 43. Martin M. Cutadapt removes adapter sequences from high-throughput sequencing reads.
681 EMBnet J. 2011;17:pp–10.

682 44. Dobin A, Gingeras TR. Mapping RNA-seq Reads with STAR: Mapping RNA-seq Reads with STAR. In:
683 Bateman A, Pearson WR, Stein LD, Stormo GD, Yates JR, editors. Curr Protoc Bioinforma [Internet].
684 Hoboken, NJ, USA: John Wiley & Sons, Inc.; 2015 [cited 2017 Jan 9]. p. 11.14.1-11.14.19. Available
685 from: http://doi.wiley.com/10.1002/0471250953.bi1114s51

686 45. Wang L, Wang S, Li W. RSeQC: quality control of RNA-seq experiments. Bioinforma Oxf Engl.
687 2012;28:2184–5.

688 46. Anders S, Pyl PT, Huber W. HTSeq--a Python framework to work with high-throughput sequencing
689 data. Bioinformatics. 2015;31:166–9.

690 47. Love MI, Huber W, Anders S. Moderated estimation of fold change and dispersion for RNA-seq
691 data with DESeq2. Genome Biol [Internet]. 2014 [cited 2017 May 31];15. Available from:
692 http://genomebiology.biomedcentral.com/articles/10.1186/s13059-014-0550-8

693 48. Love MI, Anders S, Kim V, Huber W. RNA-Seq workflow: gene-level exploratory analysis and
694 differential expression. F1000Research. 2016;4:1070.

695 49. Wickham H. Ggplot2: elegant graphics for data analysis. New York: Springer; 2009.

696 50. Yu G, Wang L-G, Han Y, He Q-Y. clusterProfiler: an R Package for Comparing Biological Themes
697 Among Gene Clusters. OMICS J Integr Biol. 2012;16:284–7.

698 51. Carlson M. org.At.tair.db: Genome wide annotation for Arabidopsis. 2018.

699

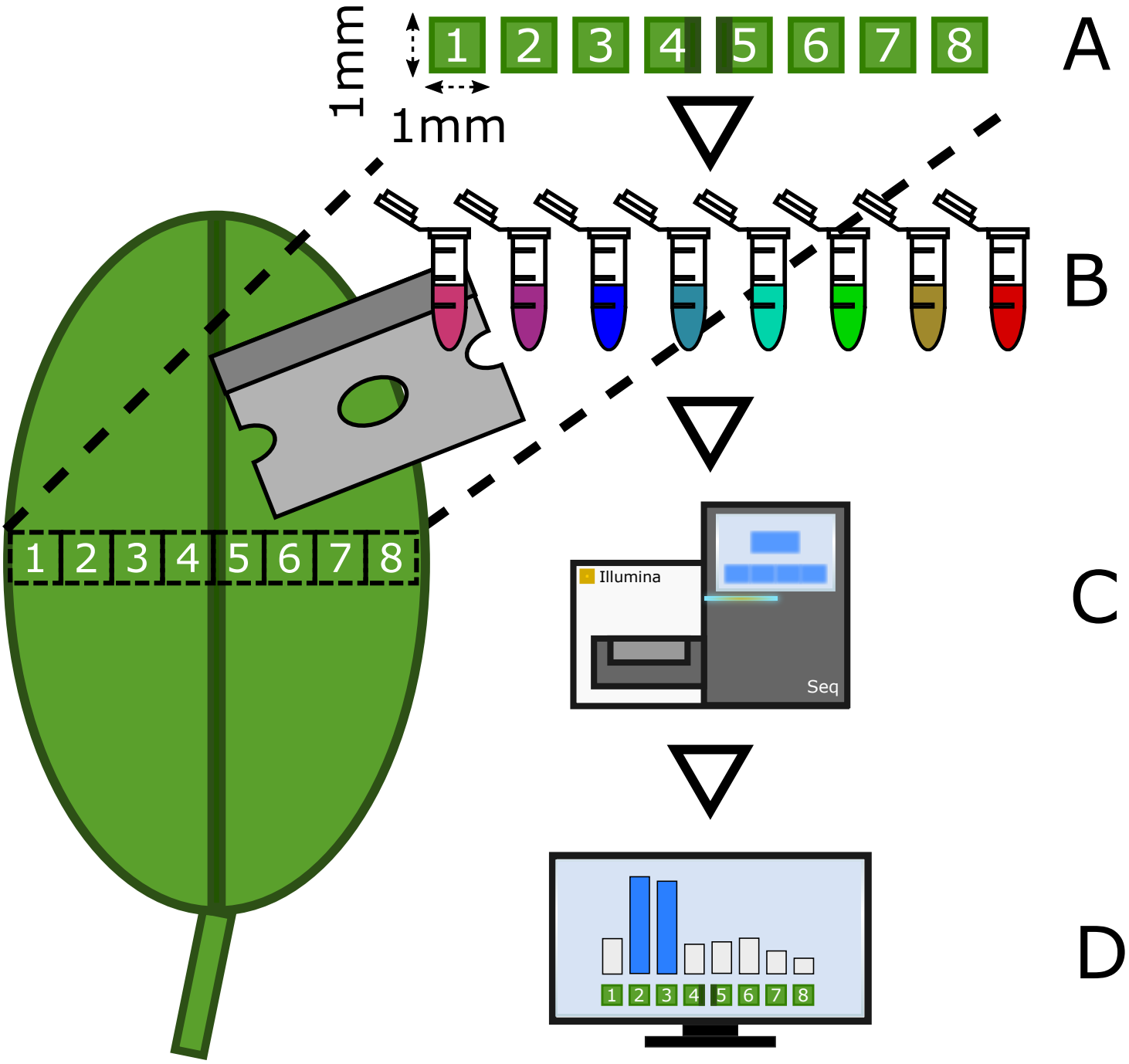
1mm
1mm
1 2 3 4 5 6 7 8
A
B
1 2 3 4 5 6 7 8
Illumina
Seq
C
1 2 3 4 5 6 7 8
D

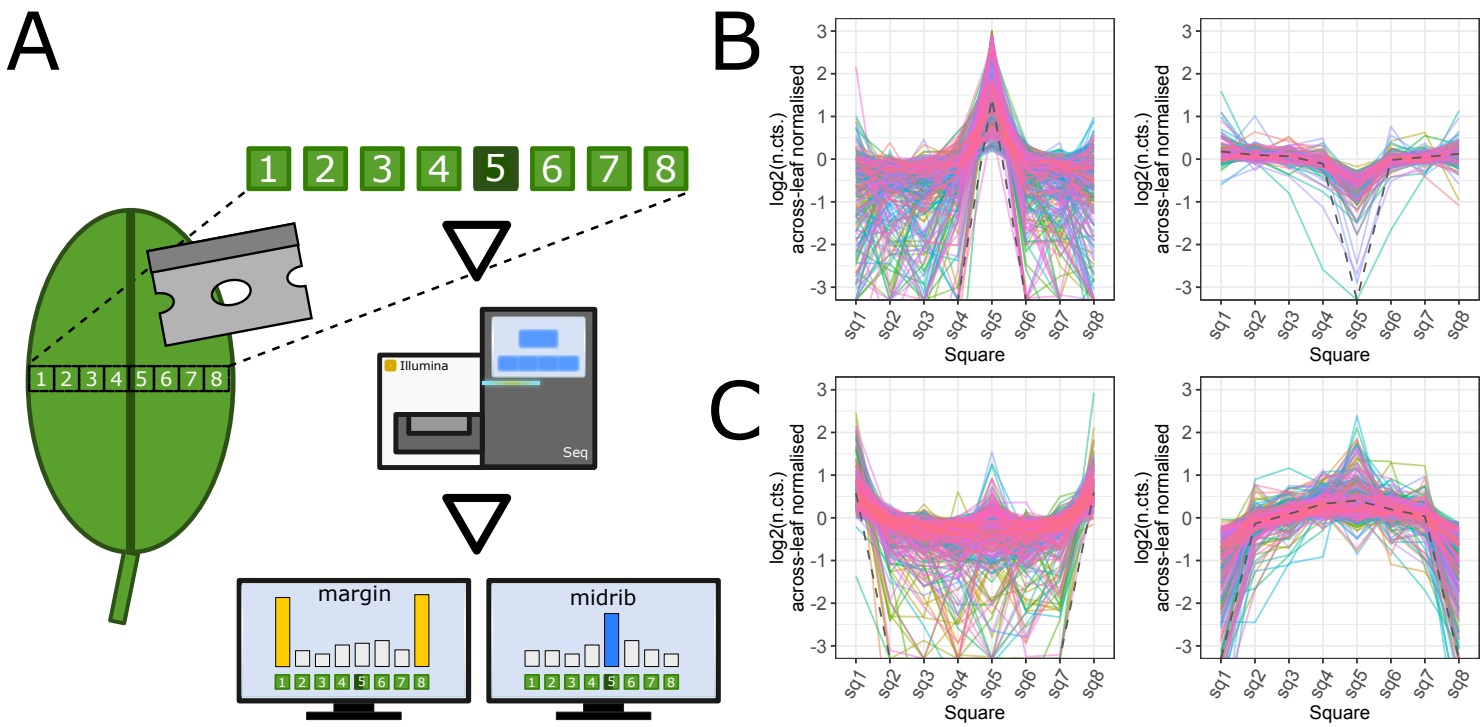
A
1 2 3 4 5 6 7 8
1 2 3 4 5 6 7 8
Illumina
Seq
margin
midrib
B
C
log2(n.cts.)
across-leaf normalised
Square
sq1
sq2
sq3
sq4
sq5
sq6
sq7
sq8

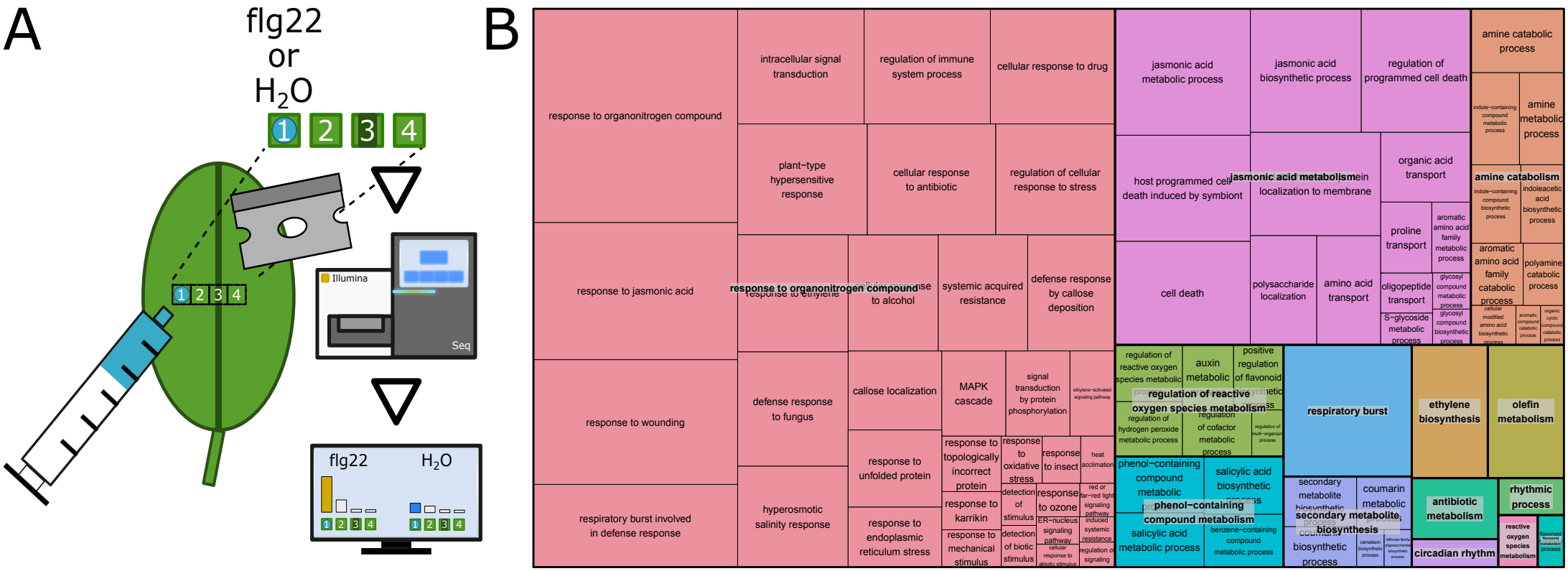
A
flg22
or
H_2O
1 2 3 4
1 2 3 4
Illumina
Seq
flg22
H_2O
1 2 3 4
1 2 3 4
B
response to organonitrogen compound
intracellular signal transduction
regulation of immune system process
cellular response to drug
plant−type hypersensitive response
cellular response to antibiotic
regulation of cellular response to stress
response to jasmonic acid
response to organonitrogen compound
response to ethylene
response to alcohol
systemic acquired resistance
defense response by callose deposition
response to wounding
defense response to fungus
callose localization
MAPK cascade
signal transduction by protein phosphorylation
ethylene−activated signaling pathway
response to unfolded protein
response to topologically incorrect protein
response to oxidative stress
response to insect
heat acclimation
response to karrikin
detection of stimulus
response to ozone
red or far−red light signaling pathway
ER−nucleus signaling pathway
induced systemic resistance
response to endoplasmic reticulum stress
response to mechanical stimulus
detection of biotic stimulus
cellular response to abiotic stimulus
regulation of signaling
respiratory burst involved in defense response
hyperosmotic salinity response
jasmonic acid metabolic process
jasmonic acid biosynthetic process
regulation of programmed cell death
host programmed cell death induced by symbiont
jasmonic acid metabolism
protein localization to membrane
organic acid transport
proline transport
aromatic amino acid family metabolic process
cell death
polysaccharide localization
amino acid transport
oligopeptide transport
glycosyl compound metabolic process
S−glycoside metabolic process
glycosyl compound biosynthetic process
amine catabolic process
indole−containing compound metabolic process
amine metabolic process
amine catabolism
indole−containing compound biosynthetic process
indoleacetic acid biosynthetic process
aromatic amino acid family catabolic process
polyamine catabolic process
cellular modified amino acid biosynthetic process
aromatic compound catabolic process
organic cyclic compound catabolic process
regulation of reactive oxygen species metabolic process
auxin metabolic process
positive regulation of flavonoid biosynthetic process
regulation of reactive oxygen species metabolism
regulation of hydrogen peroxide metabolic process
regulation of cofactor metabolic process
regulation of multi−organism process
respiratory burst
ethylene biosynthesis
olefin metabolism
phenol−containing compound metabolic process
salicylic acid biosynthetic process
phenol−containing compound metabolism
salicylic acid metabolic process
benzene−containing compound metabolic process
secondary metabolite biosynthetic process
coumarin metabolic process
secondary metabolite biosynthesis
coumarin biosynthetic process
camalexin biosynthetic process
raffinose family oligosaccharide biosynthetic process
antibiotic metabolism
rhythmic process
circadian rhythm
reactive oxygen species metabolism
flavonoid flavonoid metabolism process

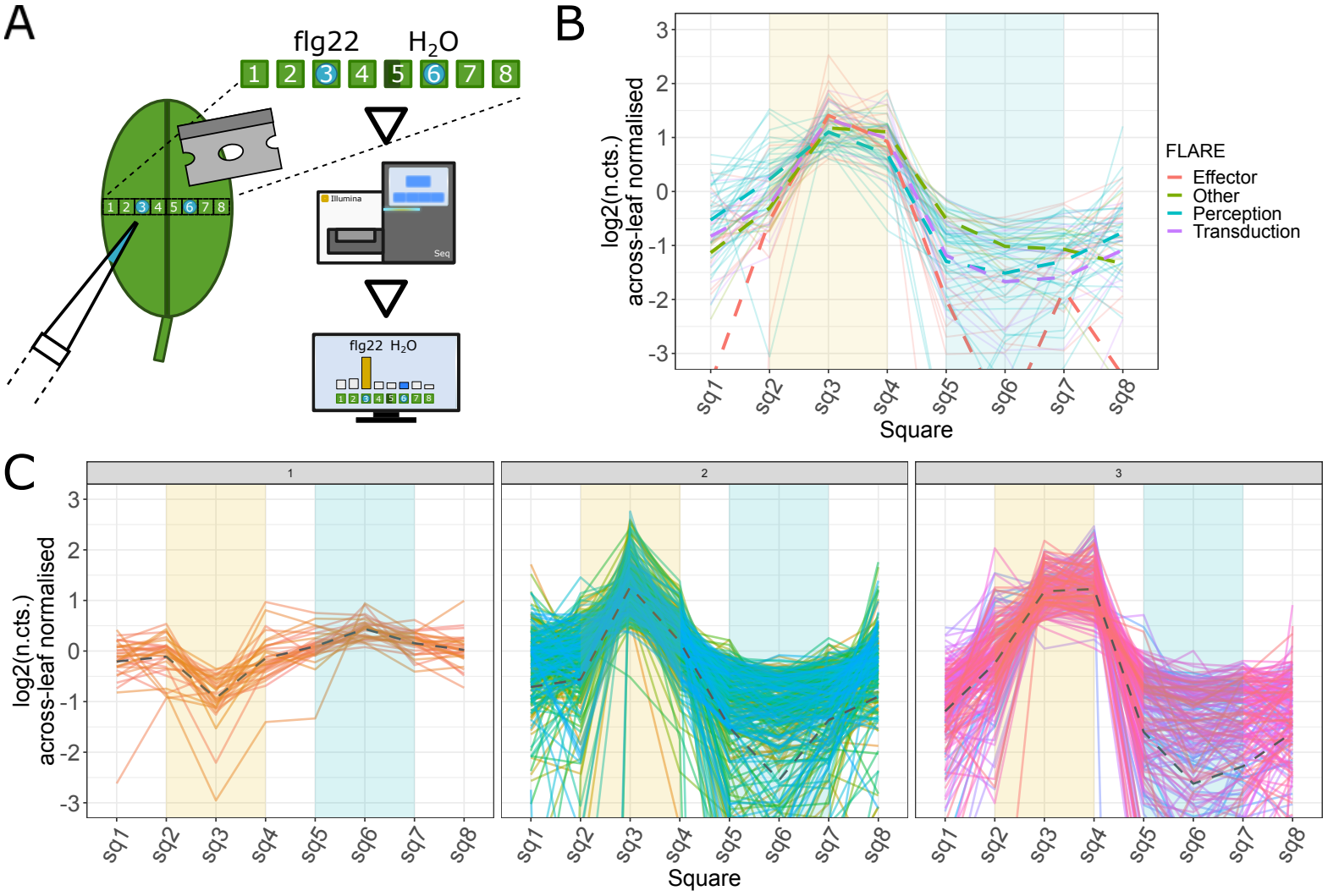
A
flg22
H_2O
1 2 3 4 5 6 7 8
Illumina
Seq
flg22 H_2O
B
log2(n.cts.)
across-leaf normalised
Square
sq1 sq2 sq3 sq4 sq5 sq6 sq7 sq8
FLARE
Effector
Other
Perception
Transduction
C
1
2
3
log2(n.cts.)
across-leaf normalised
Square

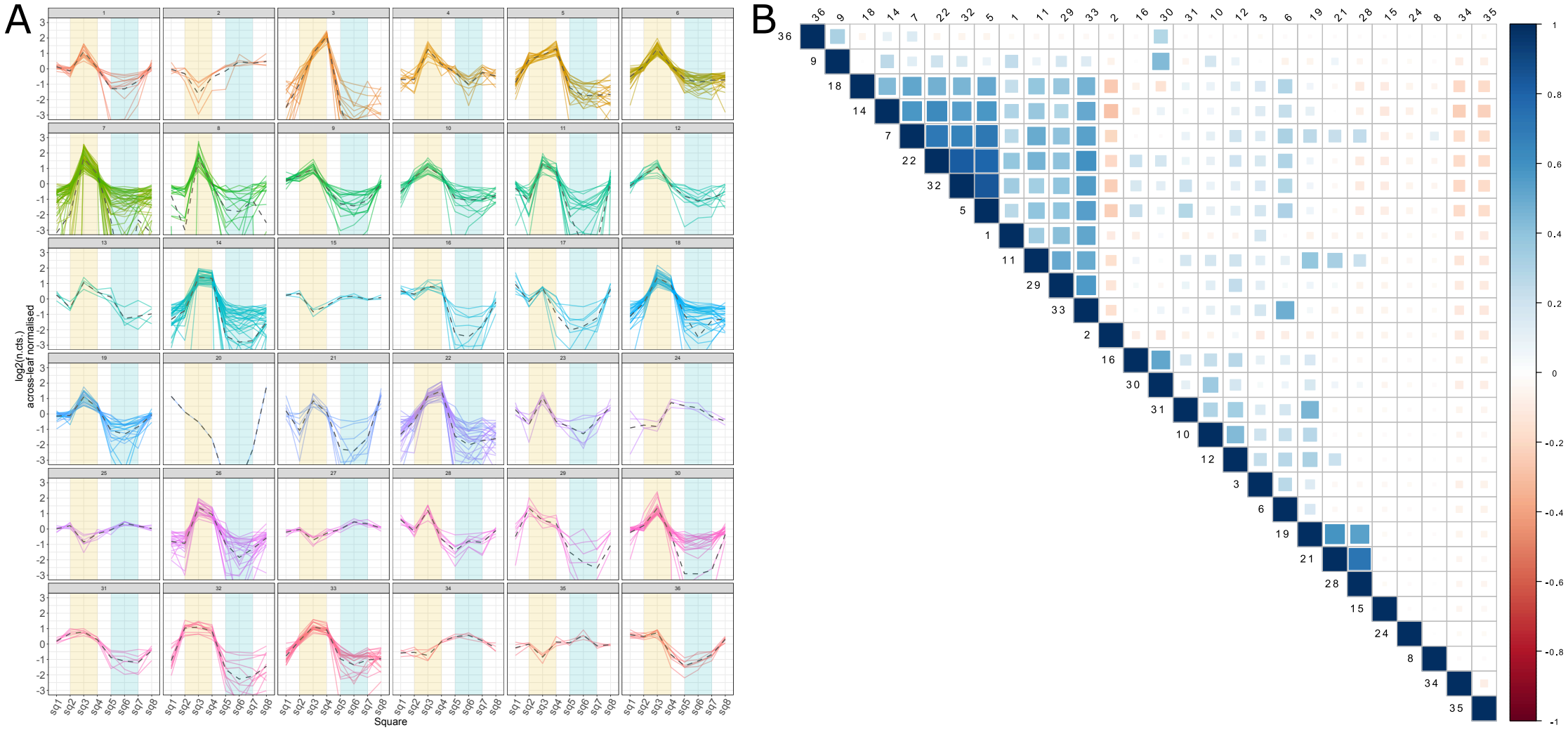
A
log2(n.cts.)
across-leaf normalised
Square
sq1
sq2
sq3
sq4
sq5
sq6
sq7
sq8
B
36
9
18
14
7
22
32
5
1
11
29
33
2
16
30
31
10
12
3
6
19
21
28
15
24
8
34
35
1
0.8
0.6
0.4
0.2
0
-0.2
-0.4
-0.6
-0.8
-1